Draft version December 23, 2022
Typeset using LaTeX **twocolumn** style in AASTeX631

CO(2-1) and 1.3 mm continuum measurements of NGC 253 Center by SMA observation

Cheng-Lin Liao,[1,2] Tzu-Shuan Kuo,[3] and Mei-Ni Chen[3]

[1]*Institute of Astronomy and Astrophysics, Academia Sinica, 11F of Astronomy-Mathematics Building, AS/NTU No.1, Sec. 4, Roosevelt Rd, Taipei 10617, Taiwan, ROC*

[2]*Graduate Institute of Astrophysics, National Taiwan University, Taipei 10617, Taiwan*

[3]*Department of Earth Sciences, National Taiwan Normal University, 116059 Taipei, Taiwan*

ABSTRACT

We have performed the spectroscopic observations towards the starburst galaxy NGC 253 at ∼230 GHz using the Submillimeter Array (SMA). The main purpose is to investigate the small structure of the 1.3 mm continuum and the CO(2-1) emission in the central region of NGC 253. Our continuum observations with a $\theta_{\rm maj} \times \theta_{\rm min}$=1.″39×1.″04 (P.A.=58°) synthesized beam resolved four aligned continuum cores, which are offset by the CO(2-1) emission. The observed continuum flux density is $F_{1.3\ \rm mm}$ = 0.404±0.025 Jy, which is 40% lower than the previously reported SMA measurement (Sakamoto et al. 2006) due to the lack of short baseline coverage in our observation. The spectroscopic redshift measured from the CO(2-1) emission line is $z = 0.0008 \pm 0.0001$, which is in good consistency with it measured by the hydrogen 21 cm line (Springob et al. 2005). These observations probe insight into the small structure in the central region of NGC 253.

Keywords: starburst galaxies, molecular gas, continuum, CO

1. INTRODUCTION

As galaxies form and evolve, the baryonic mass could be transferred between different phases, from gas in the interstellar medium (ISM) to stars and finally back into ISM as stars died. Galaxies with frequent mass transformation are recognized as active galaxies, or called the starburst galaxies, where the star-formation rate (SFR) could be as high as 100–1000 times it in our Milky Way at high redshift. Another definition of starburst galaxies is related to the gas depletion timescale ($t_{depl} = M_{gas}/SFR$), which quantifies the timescale of a galaxy to transfer its gas into stars. For the starburst galaxies, the gas depletion timescale could be as low as 10–100 Myr. Due to the high star-formation rate or the high star-formation efficiency of the starburst galaxies, they are usually very bright and luminous, which are good candidates for ISM studies.

Carbon monoxide ($^{12}C^{16}O$; hereafter CO) as the second abundant molecular gas is widely used to trace molecular hydrogen since the lack of permanent dipole makes molecular hydrogen undetectable though it is the most abundant molecular gas in galaxies. Emissions from different CO rotational transitions are related to different environments, with higher transition tracing colder and higher density regions, which are the cradles of stars. The 1.3 mm continuum mostly comes from dust emission, which is the re-emission of dust after absorbing the stellar light.

In this study, we selected NGC 253, the local starburst galaxy with detailed line observation by the Atacama Large Millimeter/submillimeter Array (ALMA) (Martín et al. 2021), as our target. NGC 253 is ∼ 3.5 Mpc (1″≈ 17 pc) away from us with an angular size of 27′× 6′. Due to the (relative) proximity and high luminosity, this is among the most representative case in the starburst galaxy studies. NGC 253 is an ideal prototype to study the effects of a central starburst on the dynamics because of the edge-on inclination, excitation conditions, and chemistry of the surrounding molecular gas. Given the high SFR of starburst galaxies, we can trace molecular clouds through CO(2-1) emission line in our observation. In addition, the 1.3 mm continuum emission could also be observed. Additionally, there are lots of archival data observed by several telescopes with different angular resolutions. In Sakamoto et al. (2006), a 7.5 hours observation of NGC 253 was carried out by SMA compact configuration, where they significantly detected ^{12}CO(2-1), ^{13}CO(2-1), C^{18}O(2-1), and 1.3 mm continuum.

Details of our SMA observations are introduced in Section 2. The results are presented in Section 3.

2. OBSERVATIONS

We have performed the SMA observations at ∼1 mm band towards NGC 253 in the extended array configuration on 2022 November 09 for an hour, which covered the baseline lengths of 20–150 $k\lambda$. The pointing and phase referencing centers are R.A. (J2000)=$00^{\rm h}47^{\rm m}33.2^{\rm s}$and Decl. (J2000)= −25°17′17.1″, respectively. We used the dual receivers mode supported with the SMA Wideband Astronomical ROACH2 Machine (SWARM) backend: The RxA receivers covered the frequency ranges of 207.5–219.5 GHz and 227.5–239.5 GHz in the lower and upper sidebands, respectively; the RxB receivers covered the frequency ranges of 223.5–235.5 GHz and 243.5–255.5 GHz, respectively. The intrinsic spectral

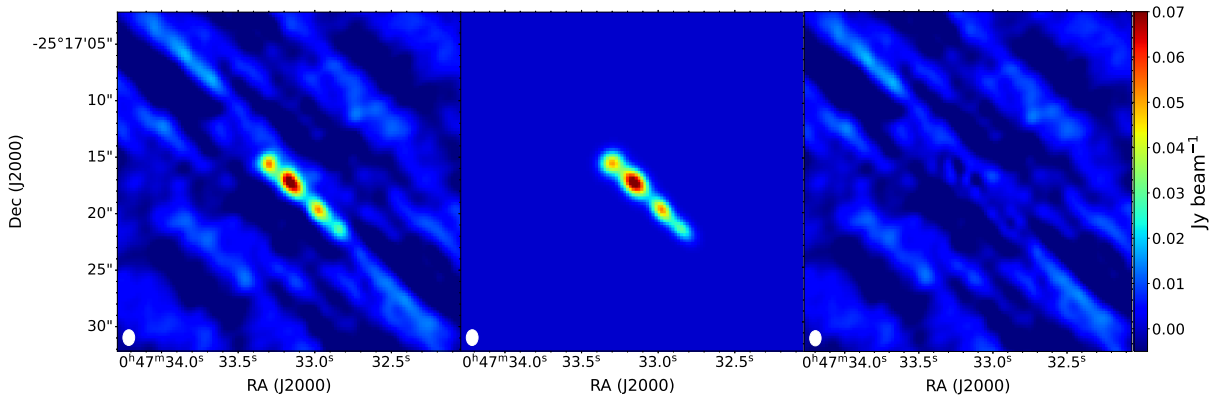

Figure 1. Left: The 1.3 mm continuum map of the central region of NGC 253. There are four cores with peak S/N $> 6\sigma$. Middle: The best-fit map, which is composed of four 2-dimensional Gaussian profiles, derived from *imfit* in CASA. Right: The residual map, which is obtained by subtracting the best-fit model from the observation. The RMS noise level of the residual map is 4.36 mJy beam^{-1}. All the plots are in units of Jy beam^{-1} as shown in the color bar.

channel width was 140 kHz. With this spectral setup, the CO(2-1) line was simultaneously covered by both the RxA and RxB receivers; the continuum emission was observed over a whole range of frequencies.

The data were manually reduced following the standard data calibration strategy of SMA. The application of Tsys information and the absolute flux, passband, and gain calibrations were carried out using the MIR IDL software package (Qi 2003). The absolute flux scalings were derived by comparing the visibility amplitudes of the gain calibrators with those of the absolute flux calibrator, Neptune. We nominally quote the ∼15% typical absolute flux calibration error of SMA.

With a total of eight antennas of SMA in our observation, we obtained 56 sets of data forming by the lsb and usb of each two antenna. In order to calibrate the observed sources, we selected 2348-165 as the gain calibrator, Neptune as the flux calibrator, and 1924-292 as the pass band calibrator. Among these, we removed the data from the RxB receivers of antenna 5 due to the failure and removed the data having elevation angle $< 25°$of the flux calibrator. Since the edge channels have some spikes caused by hardware, the first and last 500 channels of each spectral window of both RxA receivers and RxB receivers have been deleted. Then, Tsys correction is implemented. An emission line is found near the observed frequency 230 GHz, which corresponds to the spectral line of CO(2-1).

After calibration, the zeroth-order fitting of continuum levels and the joint weighted imaging of all continuum data were performed using the Miriad software package (Sault et al. 1995). We performed the zeroth-order multi-frequency synthesis (mfs) imaging by combing all available calibrated data, as shown in the left panel of Figure 1. The final continuum image was produced using Natural weighting in order to reconstruct more flux. The achieved synthesized beam size and root-mean-square (RMS) noise level are $\theta_{\rm maj} \times \theta_{\rm min}$ = 1.″39 × 1.″04 (P.A.=58°) and 4.94 mJy beam^{-1}, respectively.

3. RESULTS

3.1. *1.3 mm Continuum Emission*

We combined all the data except for the frequency where CO(2-1) is detected and obtained the 1.3 mm continuum map of the central region in NGC 253, as shown in the left panel Figure 1. The signal-to-noise ratio (S/N) of the four cores, from top-left to bottom-right, are respectively 11.1, 18.0, 11.9, and 6.6 σ. This multiple-core feature in the central region of NGC 253 was not found in previous observation in Sakamoto et al. (2006), where there is only one core found in their continuum map, due to the poor resolution. This finding infers that we are observing the high-density continuum cores, which were not detected in previous studies, in the central region of NGC 253.

We fit the continuum maps with four 2-dimensional Gaussian profiles, where the best-fit models and the residual are shown in the middle and right panel of Figure 1, respectively. The RMS noise level of the residual map is 4.36 mJy beam^{-1}, suggesting that the fitting is successful. The major axis full width at half maximum (FWHM) of the four components, from top-left to bottom-right, are 1.″25±0.″22, 1.″92±0.″20, 1.″46±0.″28, and ≤2.″1; while the FWHM of the minor axis are 0.″82±0.″38, 0.″81±0.″21, 0.″07±0.″52, and ≤0.″47. Since the fourth component is too small to resolve in our observation, the FWHM of its major and minor axis is the upper limit.

With the best-fit model, we could also estimate the peak intensity and the total flux. The best-fit peak intensity of the four components, from top-right to bottom-left, are 48.6±4.7, 78.5±4.6, 52.1±4.5, and 28.8±4.5 mJy beam^{-1}. The total flux, which is calculated by summing all the best-fit Gaussian profiles, is 0.404 ± 0.025 Jy, which is only about 40% of the total flux measured in Sakamoto et al. (2006). We note that the missing flux may be aroused from the filtered-out large-scale structure since we do not have short baselines as the observation of Sakamoto et al. (2006).

3.2. *CO(2-1) Emission*

Though having less than one-hour observation on NGC 253, we detected the CO(2-1) emission line in the central region of NGC 253. Figure 2 demonstrate the integrated flux maps, the zeroth moment map (moment 0 map), of NGC 253, with velocity integrating from −200 to 200 km/s, where the zero point velocity is set to the redshifted frequency of CO(2-1) emission line by adopting the redshift, $z = 0.00081$, measured from literature (Springob et al. 2005). There are four peaks, which are the green crosses in Figure 2, in the moment 0 map, showing the small structure of the CO molecular gas in the central region of NGC 253. Overlapping the continuum map on the moment 0 map, we found an offset between 1.3 mm continuum and CO(2-1).

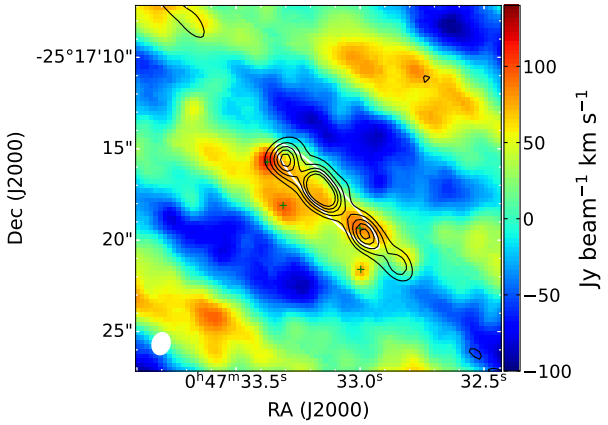

Figure 2. The CO(2-1) moment 0 map of the central region of NGC 253 (color image). The velocity integration range is from −200 to 200 km/s. The black contours are the 1.3 mm continuum emission at 3-, 5-, 7-, 9-, and 11-σ level. The white ellipse, which is the best-fit model of the continuum map fitted by one 2-dimensional Gaussian profile, demonstrates the aperture used for extracting the CO spectrum, showing in Figure 4. The green crosses show four peaks of the CO(2-1) integrated map.

We show the channel maps in Figure 3 with 10 km/s interval for each channel. There are some strong emissions can be continuously found in the channel maps, showing that they may not be artificial emissions. For example, a point-like emission exists in channels of −130 to −80 km/s, and there are some complex structures found in −20 to −40 km/s channels. However, the fringe patterns are severe in some channels because the large structure of CO(2-1) was filtered out in our observation due to the lack of short baseline coverage. We note that this issue can be solved by combining our high-resolution data with lower-resolution data from either single-dish observation or short baseline interferometry observation.

The extracted 1-dimensional spectrum of CO(2-1) is shown in Figure 4. We fit the continuum map with one 2-dimensional Gaussian profile as the aperture for

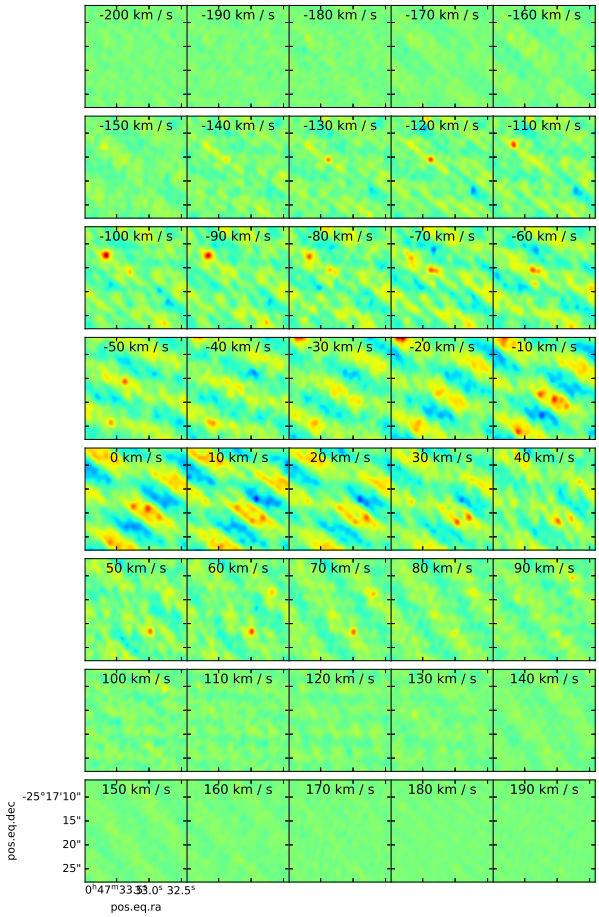

Figure 3. The zoom-in channel maps of CO(2-1) emission of NGC 253 with 10 km/s interval. Each box is in the size of 20" × 20" (∼ 340pc×340pc). Fringe patterns are clear in some middle channels due to the lack of short baselines to cover large-scale structure emissions.

extracting the spectrum. The best-fit of the continuum map is the white ellipse shown in Figure 2, which is centered at R.A. (J2000)=$00^h47^m33.132^s$and Decl. (J2000)= $-25°17'17.606''$with major and minor FWHM of $7.''90$ and $1.''47$ and position angle of 45.63°. The 1-dimensional spectrum, which is the blue step in Figure 4, is mainly composed of a central peak emission at $\nu \approx 230.35$ GHz and two minor emissions around it. To specify the central frequency of CO(2-1), we fit a Gaussian profile, Flux=A×exp$(-(\nu-\mu)^2/2\sigma)$, where A is the amplitude, μ is the central frequency, and σ is the standard deviation. The best-fit parameters and the corresponding uncertainties are shown in the legend in Figure 4. With the standard deviation from the best-fit parameter, the FWHM of the CO(2-1) emission is 92 ± 6 km/s, which is about 2 times smaller than what Sakamoto et al. (2011) estimated (FWHM= 167 ± 8 km/s). We note that the smaller line width we obtained compared to literature measurements is due to the lack of extended emission data. Namely, what we measured is

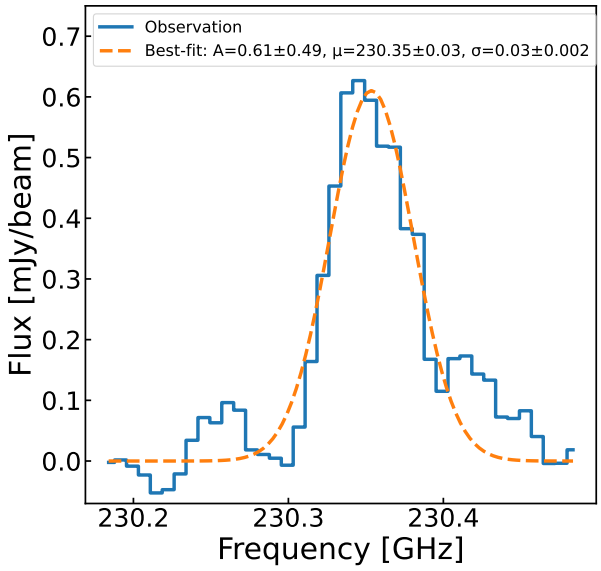

Figure 4. CO(2-1) line profile extracted from the region shown as the white ellipse in Figure 1. The best-fit Gaussian profile is plotted as the orange dashed line, where the best-fit parameters and the corresponding uncertainties are in the legend box.

the central core profile. Besides, with the best-fit central frequency of CO(2-1), we derived the redshift of NGC 253 as $z = 0.0008 \pm 0.0001$, which is consistent to the value ($z = 0.000807 \pm 0.000002$) measured by atomic hydrogen presented in Springob et al. (2005).

The Submillimeter Array is a joint project between the Smithsonian Astrophysical Observatory and the Academia Sinica Institute of Astronomy and Astrophysics, and is funded by the Smithsonian Institution and the Academia Sinica (Ho et al. 2004).

Facilities: SMA

Software: astropy (Astropy Collaboration et al. 2013), Numpy (van der Walt et al. 2011), APLpy (Robitaille & Bressert 2012), MIR IDL (Qi 2003), Miriad (Sault et al. 1995), CASA (McMullin et al. 2007),

REFERENCES

Astropy Collaboration, Robitaille, T. P., Tollerud, E. J., et al. 2013, A&A, 558, A33, doi: 10.1051/0004-6361/201322068

Ho, P. T. P., Moran, J. M., & Lo, K. Y. 2004, ApJL, 616, L1, doi: 10.1086/423245

Martín, S., Mangum, J. G., Harada, N., et al. 2021, A&A, 656, A46, doi: 10.1051/0004-6361/202141567

McMullin, J. P., Waters, B., Schiebel, D., Young, W., & Golap, K. 2007, Astronomical Society of the Pacific Conference Series, Vol. 376, CASA Architecture and Applications, ed. R. A. Shaw, F. Hill, & D. J. Bell, 127

Qi, C. 2003, in SFChem 2002: Chemistry as a Diagnostic of Star Formation, ed. C. L. Curry & M. Fich, 393

Robitaille, T., & Bressert, E. 2012, APLpy: Astronomical Plotting Library in Python, Astrophysics Source Code Library, record ascl:1208.017. http://ascl.net/1208.017

Sakamoto, K., Mao, R.-Q., Matsushita, S., et al. 2011, ApJ, 735, 19, doi: 10.1088/0004-637X/735/1/19

Sakamoto, K., Ho, P. T. P., Iono, D., et al. 2006, ApJ, 636, 685, doi: 10.1086/498075

Sault, R. J., Teuben, P. J., & Wright, M. C. H. 1995, in Astronomical Society of the Pacific Conference Series, Vol. 77, Astronomical Data Analysis Software and Systems IV, ed. R. A. Shaw, H. E. Payne, & J. J. E. Hayes, 433. https://arxiv.org/abs/astro-ph/0612759

Springob, C. M., Haynes, M. P., Giovanelli, R., & Kent, B. R. 2005, ApJS, 160, 149, doi: 10.1086/431550

van der Walt, S., Colbert, S. C., & Varoquaux, G. 2011, Computing in Science and Engineering, 13, 22, doi: 10.1109/MCSE.2011.37